

VECTOR WIND, HORIZONTAL DIVERGENCE, WIND STRESS AND WIND STRESS CURL FROM
SEASAT-SASS AT A ONE DEGREE RESOLUTION

By

Willard J. Pierson Jr. ⁺, Winfield B. Sylvester ⁺ and Robert E. Salfi ^{*}

+The City College of New York, N. Y., N.Y. 10031

*Present affiliation, Hofstra University, Hempstead, N.Y. 11550

ABSTRACT

Conventional data obtained in 1932 are contrasted with SEASAT-SASS and SMMR data to show how observations at a single station can be extended to an area of about 150,000 square km by means of remotely sensed data obtained in nine minutes. Superobservations at a one degree resolution for the vector winds are estimated along with estimates of their standard deviations. From these superobservations, the horizontal divergence, vector wind stress, and the curl of the wind stress can be found.

INTRODUCTION

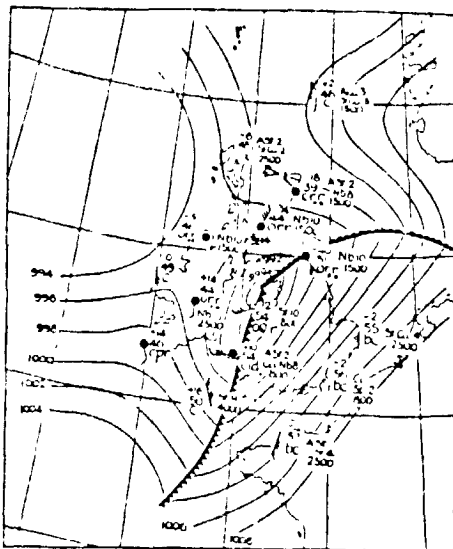
The basic tenets of those who believe that it is possible to predict the weather are three. These are (1) that the time evolution of the meteorological variables can be correctly described by appropriate equations, (2) that the initial conditions for the start of the prediction can be adequately specified and (3) that computers can be made with a large enough capacity and a fast enough speed to compute the evolution of the weather for the future. These tenets evolved with time from the days of Bjerknes (1904) who wrote that what was needed was "a sufficiently accurate knowledge of the state of the atmosphere at the initial time" and "a sufficiently accurate knowledge of the laws according to which one state of the atmosphere develops from another", through Richardson's (1922) "Weather Prediction by Numerical Process", on to the day when the authors of a recent paper wrote "The main reason we cannot tell the weather tomorrow is that we do not know the weather today".

These tenets are interdependent because improved computers provide higher resolution. Improved descriptions of the physics of the atmosphere require more data. The problem is to predict the synoptic scale meteorological evolution and to filter out the higher wavenumbers and frequencies. This is a corollary of the basic tenets and involves all aspects of turbulence, where much is yet to be learned.

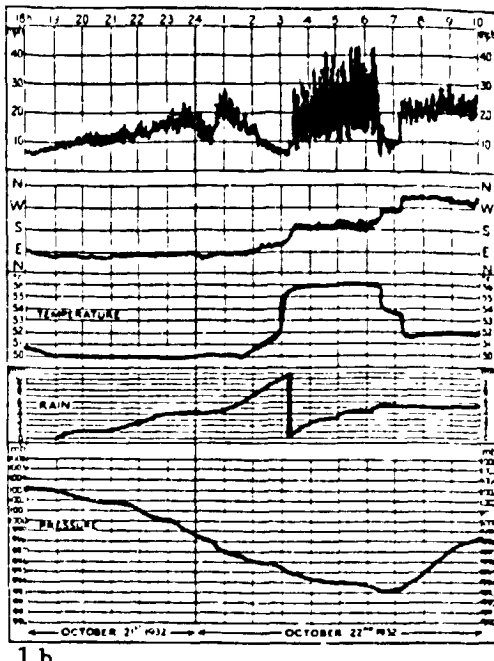
Much of what has been learned in the past about the behaviour of weather systems has been lost because of present day computer constraints. To our knowledge, no operational hemispheric numerical model with a one degree by one degree resolution, and a corresponding vertical resolution, presently exists. With an adequate description of the physics of the atmosphere and of subgrid turbulence, including the possibility of transfer of energy from high to low wave numbers, a one degree, at least hemispheric model, is presently conceivable.

OCTOBER 21, AND 22, 1932 AT HOLYHEAD, ENGLAND

Before showing what can be achieved by means of remote sensing, it is useful to go back to a text by Brunt (1942). It is then possible to compare the results of the analysis of SEASAT data obtained in about 9 minutes with data obtained over a 16 hour period in England.



The Depression of October 22, 1932, at 07h



1 b

Fig. 1(a) Synoptic analysis for the weather on October 22, 1932 at 0700 for the British Isles and part of Europe and (b) time histories at Holyhead. Wind speed from 0 to 50 miles per hour; Direction, meteorological convention; Temperature, degrees Fahrenheit 50° to 58°; Integrated rainfall in millimeters, 0 to 10 mm; Sea level pressure, millibars, 990 to 1006. From Brunt (1942).

Fig. 1(a) shows the synoptic scale analysis for 07h Oct. 22, 1932, London time, for an area around the British Isles. Fig. 1(b) shows the time history of the evolution of winds, temperature, integrated rainfall and sea surface atmospheric pressure at Holyhead, England (approximately 52.5°, 4.8° W) beginning on Oct. 21 at 18h and ending on Oct 22 at 10h (16 hours). Some data have probably been omitted for clarity in Fig. 1(a) but there are roughly four observations per 10 degree latitude by longitude "square" which permit an adequate analysis. The cold front of the open wave cyclone is in the process of passing Holyhead.

The anemometer had a rather short time constant so that mesoscale fluctuations of the wind were recorded. Even in 1932, it would have been obvious that a two minute average could give erroneous synoptic scale values as recently rediscovered by Pierson, et al. (1980) and made quantitative by Pierson (1983a).

If one imagines the wave cyclone to be moving without too much change in form along an appropriate track, the winds in advance of the warm sector were ENE for the first eight hours building from 6 or 7 miles per hour (2.24 mph equals 1 m/s) to 22 mph (with gusts to 29) followed by a decrease to 6 mph and a wind shift to the ESE. The wind shift to SSW occurred in about 20 minutes. The temperature rose slowly from about 1:40 to 3 AM then rapidly for 10 to 15 minutes with a $1 - \exp(-Bt)$ asymptotic approach to 56° F. The total warming was 6° F.

The winds in the warm sector were very gusty and turbulent with 40° fluctuations in direction and speeds that varied moment by moment from under 10 mph to nearly 45 mph. The average wind in the warm sector increased from about 20 mph to 25 mph before the cold front passage.

The cold front went by in two steps at about 6:30 and 7:20 with a wind shift to the WSW followed by the final one to the NW. The temperature dropped sharply twice in 2° F steps and settled down to a value of 52° F.

Light pre-warm front rain occurred from 1900 to 1930 and from 2050 to 2255. Heavier rain began after midnight and lasted steadily for more than two hours tapering off after the warm front passage and stopping at about 0620 at the first

passage of the cold front.

With modern communication systems, it would be possible, in principle, to obtain similar data with data buoys over the ocean and closely spaced land installations for pre processing locally to define the planetary boundary layer with sufficient accuracy at the synoptic scale and to collect and use the data in time for forecasts. The cost would be substantial. Over the oceans, remote sensing can provide a cost effective alternative.

THEORY

To predict the weather, meteorologists start with the hydrodynamic equations for a rotating Earth plus H_2O conservation equations, sources and sinks, plus radiation budget equations, plus whatever else might be needed and try to put them in a form that can be integrated forward by means of about 10 minute time steps so as to reach out to the future. The first difficulty is that the hydrodynamic equations are inappropriate. It is impossible to measure the various fields at the resolutions they need, and equally impossible to integrate them forward in time to make a forecast. The atmosphere is turbulent at scales that are, and always will be, unresolvable for such purposes. The equations that are actually used require time and space averaged values and therefore become strangely altered because they must account for the effects of fluctuations within the space and time average. A host of new terms such as $-\langle u'w' \rangle$ arise because of nonlinearity that must be removed by means of an appropriate closure model. Just how this ought to be done is a matter for discussion as in Robinson (1978), among others.

To put things simply, the synoptic scale winds are needed for a numerical weather prediction as defined in a circular way by Pierson (1983a). Each SASS wind in a swath is defined by four numbers; they are the latitude, θ_i , longitude λ_i , wind speed at 19.5 meters for an effective neutral wind $|V|_i$, and the meteorological wind direction, x_i , after the removal of ambiguities.

Each SASS wind in a data set departs from the desired synoptic scale value at θ_i , x_i for two reasons (at least). The footprint (or cell) illuminated by the radar is analogous to a rather brief time average that would not quite recover the synoptic scale value. For a typical cell size and a synoptic scale wind of 15 m/s the variability due to this effect can, for example, be ± 0.38 m/s at one standard deviation. Other sources of error caused by the radar itself, and lumped into one term (Pierson(1983(a), 1983(b)), produce about an 0.6 m/s variation, but this can vary for various reasons as a function of the wind direction and incidence angle. For direction, the corresponding values are 1.2° and 6° for this example. The combined effect is about 0.71 m/s for speed and slightly over 6° for direction. These are representative conditions, but over a full swath these two effects can combine to give variations more than twice as large or less than half as much. They are inseparable after the vector wind is found. Neither effect is desirable for the purpose of synoptic scale analyses. Both are random from one measurement to another.

The data analysis procedure reduces these sources of variability and recovers a reliable estimate (in a statistical sense) of the synoptic scale wind at 19.5 m above the sea surface for a neutrally stratified atmosphere. For each integer value of latitude and longitude in the swath, say θ_o , λ_o , all SASS wind within the 2 by 2 degree "square" surrounding the target point were found. The average latitude and longitude of the SASS winds in this sample would not quite be at θ_o , λ_o and a few values were dropped from the sample at the outer edges to obtain an average latitude and longitude close to θ_o , λ_o . This slightly reduced sample was then processed as a superobservation to obtain synoptic scale fields with estimates of sampling variability effects at a one degree resolution by overlapping the 2 by 2 degree squares.

For each sample a mean direction can be found as in (1).

$$\bar{x} = \frac{1}{N} \sum x_i \quad (1)$$

Each SASS wind can be resolved into components parallel and normal to \bar{x} such as v_{pi} and v_{Ni} such that

$$\bar{v}_p = \frac{1}{N} \sum v_{pi} \quad (2)$$

and $\bar{v}_N = \frac{1}{N} \sum v_{Ni} \quad (3)$

and their variances can be found as in (4) and (5). Also quantities such as $\sum(\theta_i - \theta_o) = \sum \Delta \theta_i$, $\theta_o + \Delta \theta$, $\lambda_o + \Delta \lambda$, VAR ($\Delta \theta$), and so on, are needed because the winds are not exactly at λ_o , θ_o .

$$\text{VAR } \bar{v}_p = \frac{1}{N} \sum (v_{pi} - \bar{v}_p)^2 \quad (4)$$

$$\text{VAR } \bar{v}_N = \frac{1}{N} \sum (v_{Ni} - \bar{v}_N)^2 \quad (5)$$

From standard statistical theory, the expected value of the mean is the mean and the variance of the mean is the variance of the sample as in (4) and (5) times N^{-1} . The only difficulty is the presence of gradients in the winds over the swath which can overestimate the variances that are needed and the slight mis-location of the desired winds by $\Delta \theta$, $\Delta \lambda$.

Further data processing in terms of east-west components, U_λ and north-south components, V_θ , allows the effects of gradients to be removed to first order, the wind vector to be located at λ_o , θ_o , and the standard deviations of the mean east-west and north-south components to be found. The final results, with added complexities at the edges of the available data, were values for the vector components of the wind at each θ_o , λ_o that were much more accurate estimates of the synoptic scale wind with known effects of sampling variability as in equations (6) and (7). (We have simplified notation for this paper).

$$U_{\lambda s} = \bar{U}_\lambda + t_1 \Delta U_1 + t_2 \Delta U_2 \quad (6)$$

$$V_{\theta s} = \bar{V}_\theta + t_1 \Delta V_1 + t_2 \Delta V_2 \quad (7)$$

In (6) and (7), $U_{\lambda s}$ and $V_{\theta s}$ are the desired, but always unknown, synoptic scale values, \bar{U}_λ and \bar{V}_θ are their superobservation estimates and ΔU_1 , ΔU_2 , ΔV_1 , ΔV_2 , express the reduced effects of the components of (4) and (5) after removing the contribution from gradients in the wind field and obtaining the appropriate vector components. The values of t_1 and t_2 near the middle of the swath where N can be above 30 are close to being values drawn at random from a zero mean unit variance normal probability density function.

As an example, at 54° N 209° W (for another SEASAT pass), the superobservation yielded a wind from 260° at 20.2 m/s. The other data obtained then gave (8) and (9) in m/s. From (8) and (9), as one of many examples that could be given, the uncertainty in wind speed is ± 0.17 m/s at one standard deviation and the uncertainty in direction is $\pm 2.75^\circ$. It will be a while before meteorologists will believe such results.

$$U_{\lambda s} = 19.95 + t_1(0.17) + t_2(0.14) = 19.95 + t_1^*(0.22) \quad (8)$$

$$V_{\theta s} = 0.156 + t_1(0.02) + t_2(-0.96) = 0.156 + t_2^*(0.96) \quad (9)$$

By these methods as an example for the REV to be studied, the original 1,081 SASS winds were reduced to 120 superobservation winds as in (6) and (7) with each wind accompanied by estimates of its sampling variability for a reduction to 11% of the original data for further processing.

For every point in the superobservation wind field that had four points around it, it was possible to estimate the horizontal field of divergence at 19.5 meters and to carry along the four terms in (6) and (7) so as to obtain the standard deviation of the estimate of the divergence. The appropriate equation is (10)

$$\text{div}_2 \vec{W}_h = \frac{1}{R \cos \theta} \left(\frac{\partial U_\lambda}{\partial \lambda} + \cos \theta \frac{\partial V_\theta}{\partial \theta} - V_\theta \sin \theta \right) \quad (10)$$

where R is the radius of the Earth.

The finite difference form is (11).

$$\text{div}_2 (\vec{W}_h (\theta_o, \lambda_o))_s = \frac{2.5 \cdot 10^{-6}}{\cos \theta} \left\{ (U_{s\lambda} (\theta_o, \lambda_o + 1) - U_{s\lambda} (\theta_o, \lambda_o - 1)) \right. \\ \left. + \cos \theta (V_{s\theta} (\theta_o + 1, \lambda_o) - V_{s\theta} (\theta_o - 1, \lambda_o)) \right. \\ \left. - 0.0349065 \sin \theta_o V_{s\theta} (\theta_o, \lambda_o) \right\} \quad (11)$$

Five different terms such as (8) and (9) are needed. The expected value of the 10 different terms that enter is zero so that the expected value of the divergence can be found.

Also

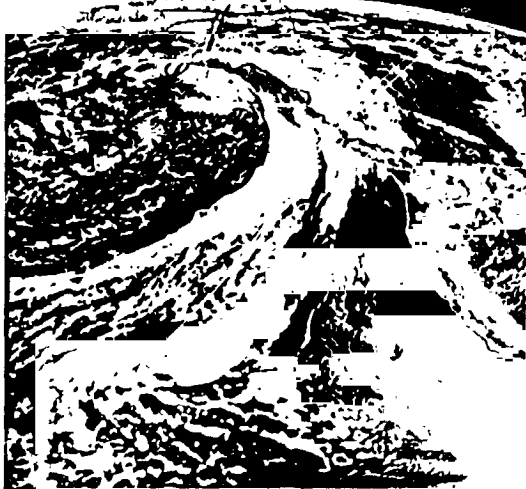
$$\mathcal{E} ((\text{div}_2 \vec{W}_h (\theta_o, \lambda_o))_s - \text{div}_2 (\vec{W}_h (\theta_o, \lambda_o)))^2 = \text{VAR}(\text{div}_2 (\vec{W}_h (\theta_o, \lambda_o))) \quad (12)$$

can be found as a weighted sum of the squares of the ΔU_j and ΔV_j so that the standard deviation of the estimate of the divergence can also be estimated. The field of horizontal divergence is rarely calculated from conventional data because of large errors in measurement. The divergences that were found formed logical coherent patterns.

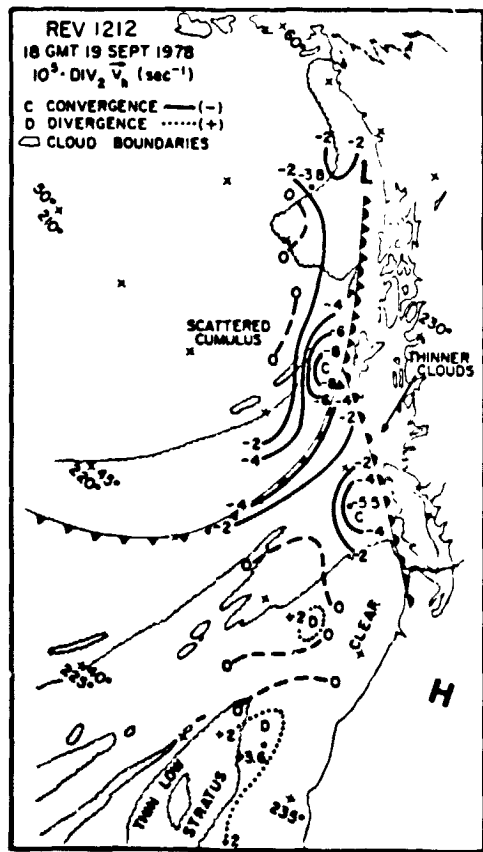
THE WESTERN NORTH PACIFIC FOR SEPTEMBER 19, 1978 AT ABOUT 1800 GMT

On this date, SEASAT crossed the Equator, on its 1212th revolution of the Earth in a retrograde circular orbit with a period of about 100 minutes at an altitude of 800 km., going north bound, a few seconds before 1754 GMT and obtained the data that were analysed for the following material between about 1803 and 1812 GMT from the SASS and the SMMR. For details, see for example *IEEE J. Oceanic Eng.* Vol. OE-5 and *J. Geophys. Res.* Vol. 87, No. C5 and Vol. 88, No. C3. Further details on these particular results and for three additional weather patterns are given by Pierson, et al. (1983). During this 9 minute interval, the SASS found 1,081 values for the winds over an area about 600 km wide extending from 35° N to 60° N in a one side scanning mode. The SMMR also obtained data over a slightly narrower swath. At nearly the same time, the GOES spacecraft obtained both visible and infrared imagery. The results for the synoptic scale wind field and the field of the horizontal divergence of the wind will be described. Fields for the wind stress, $(u^*)^2$, and the curl of the wind stress will be found by similar methods, also.

McMurdie and Katsaros (1983) have used the SMMR data to obtain the values in Fig. 3 for this REV. Their results can be combined with the vector wind values and the divergence field to produce data over an area of roughly 150,000 square kilometers that are effectively the equivalent of having records similar to Fig. 1(b) from every one degree latitude longitude intersection in the swath for synoptically averaged winds and for the rainfall rates. Given the few ship reports of sea surface atmospheric pressure within the swath, it ought not to be unduly difficult to recover the sea surface pressure field within the swath. Air temperature just above the sea surface is still a problem for remote sensing, and the sparsity of conventional ship reports makes such data difficult to obtain.



2 a



2 c

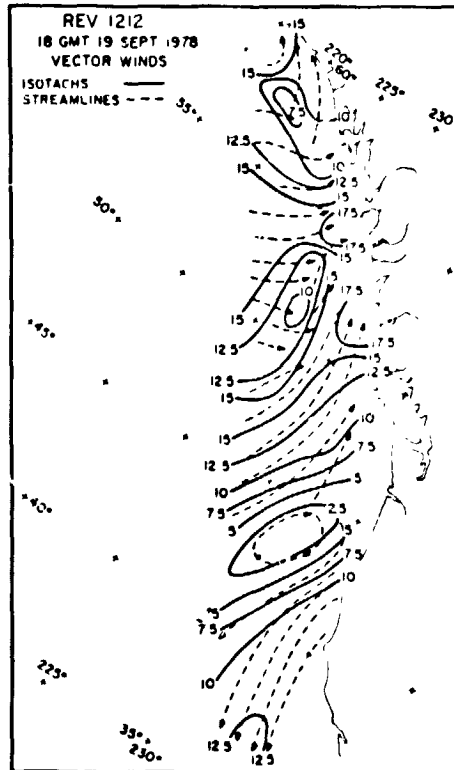


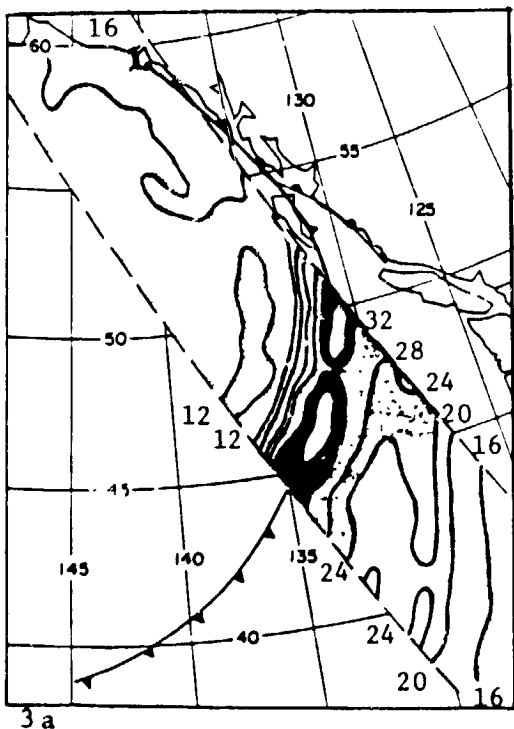
Fig. 2. (a) Geostationary cloud image of the extratropical cyclone for SEASAT REV 1212. (b) Streamline, isotach analysis of the superobservations. Speeds in meters per second. Data from the SEASAT A Scatterometer, (SASS). (c) Field of horizontal divergence computed from the superobservations. Fig. 2(a) is from Woiceshyn, et al. (1979).

The GOES cloud imagery, the SASS superobservation winds, and the divergence field computed therefrom plus the SMMR results provide a detailed meteorological description of an occluded cyclone approaching the west coast of North America. The GOES cloud image in Fig. 2(a) shows an occluded low crossing the west coast of North America. A long cold front trails to the south and west over the Pacific. The cloud shield extends well into Canada and covers Queen Charlotte Island and most of Vancouver.

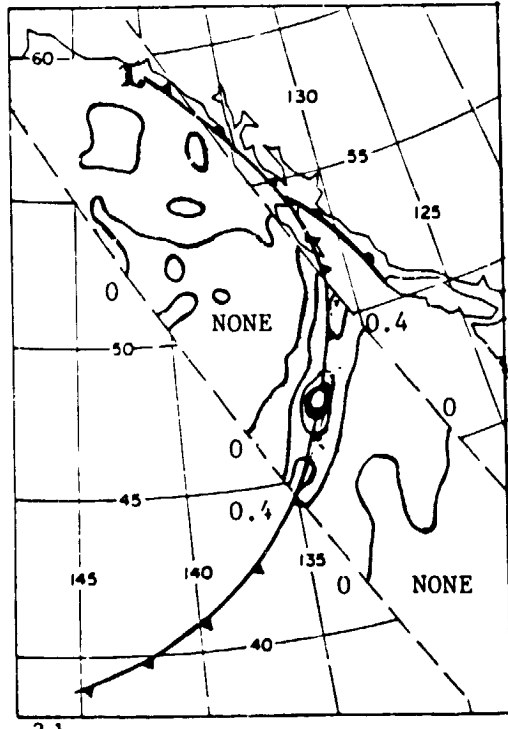
Streamlines and isotachs (m/s) are shown in Fig. 2(b). Strong warm air advection for the streamlines surrounded by the 15 m/s isotach and to the south to 10 m/s is shown. The wind shift in the general vicinity of the occlusion is shown.

Queen Charlotte Island is not shown for simplicity.

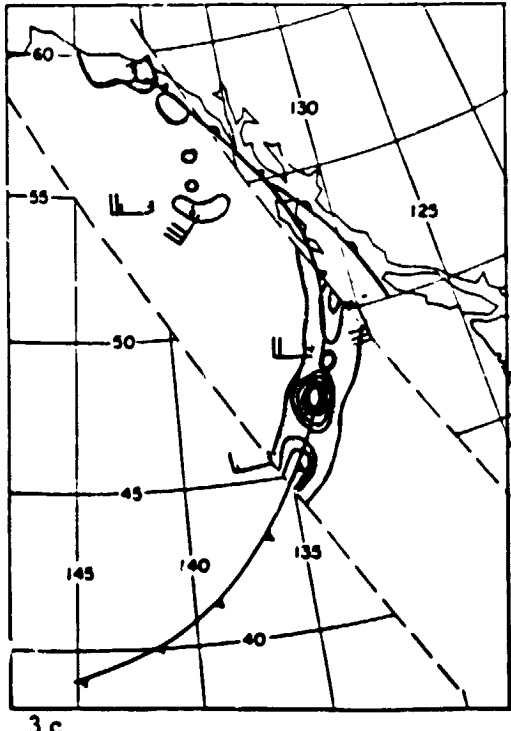
The field of divergence is shown in Fig. 2(c) based on 65 values as a composite with the frontal analysis based on conventional analysis plus a schematic of the cloud image shown in Fig. 2(a). Strong convergence is shown at the intersection of the cold and warm front with a band less than $4 \times 10^{-5} \text{ sec}^{-1}$ extending over



3 a



3 b



3 c

Fig. 3. The integrated water vapor in kg/m^2 (a), the integrated liquid water in kg/m^2 (b), and the rainfall rate in mm/hr (c), found from the Scanning Multichannel Microwave Radiometer on SEASAT. In (a) the contours that parallel the cold front have values of 16, 20, 24 and 28. The dark area has values over 32 and the inner white area values over 40. In (b), the area in the center has values of 0.8, 1.2 and 1.6 with 1.6 in white. In (c), the rainfall rate contours are for 0.4, 0.8, 1.2 and 1.6 mm/hr . with the center white dot showing 1.6 mm/hr . From McMurdie and Katsaros (1983).

more than 5° of longitude. Convergence is also shown to the west of Vancouver in the warm air sector of the system. Divergence values as high as $(3.55 \pm 0.38) \times 10^{-5} \text{ sec}^{-1}$ and as low as $(-7.98 \pm 0.91) \times 10^{-5} \text{ sec}^{-1}$ were obtained. The standard deviations show that the first was surely positive and the second surely negative. Values of near zero divergence would be indicated if the estimate plus one standard deviation and the estimate minus one standard deviation changed sign. This happened six times.

sec^{-1} and $1 \times 10^{-5} \text{ sec}^{-1}$ 28 times, suggesting

The estimate was between 1×10^{-5} and 1×10^{-5} sec $^{-1}$ areas of nearly nondivergent flow.

The higher convergence values would produce upward vertical velocities of 1.6 cm/sec at a height of 200 m. Air moving at 15 m/s will rise 57 m as it travels 54 km in one hour. Over a one degree square at 50° N about 400 cubic kilometers of air pass upward through the 200 meter level each hour in the area of strong convergence.

Figure 3 shows respectively the total mass of water vapor over each square meter of the sea surface in kg/m^2 , the total liquid water in kg/m^2 and the rainfall rate in mm/hr . The fronts in these figures are different from those in Fig. 2. The analyses involved were independent and need to be reconciled on the basis of more data and consistency checks.

These figures for REV 1212 provide valuable quantitative data on the properties of an extratropical cyclone. The winds are shown to be transporting warm moist air by means of a concentrated southerly flow in advance of the cold front. The moisture is concentrated by this flow in a narrow band along the surface front. The band of high water vapor content undoubtedly would continue beyond the swath following along the frontal system. The highest concentrations of liquid water in Fig. 3(b) are along the front and in the area of convergence of Fig. 2(b). The precipitation is patchy in small cells with values over 4 mm/hr . Were the pattern in Fig. 3(c) to be shifted north north westward, without change in form, past a point at about 49°N , 130°W , at, say, 15 or 20 m/s and the rainfall rate integrated with time, the result would be an integrated rainfall graph very similar to the one in Fig. 1(b). The cold front passage as in Fig. 1 would also appear as a time history at this and many other points properly located in time.

WIND STRESS AND WIND STRESS CURL

There are many different equations that have been proposed to relate the wind at 10 m to the wind stress defined either by

$$\vec{\tau}/\rho = u_*^2 = - \cdot u'w' \quad (13)$$

or by $C_{10} = u_*^2/\bar{U}(10)^2 \quad (14)$

as, for example, Large and Pond (1981). A completely new one based on data from three different sources was used in this study. Lots of questions in this problem are remain unsolved, but if the superobservation represents the synoptic scale wind at 19.5 meters, it can be related to the wind at 10 m by (15).

$$\bar{U}(19.5) = \bar{U}(10) + (u_*(\bar{U}(10)) \ln(19.5/10))/\kappa \quad (15)$$

and by, in meters per second,

$$u_*^2 = 10^{-3}(2.717(\bar{U}(10)) + 0.142(\bar{U}(10))^2 + 0.0761(\bar{U}(10))^3) \quad (16)$$

For selected values of $\bar{U}(19.5)$ Table 1 can be obtained as examples and as detailed a table as desired can be constructed. There is a one to one relationship between the isotach values in Fig. 2(b) and u_*^2 values from the following table and the above equations except that u_*^2 is strongly concentrated in areas of high winds. As the wind varies by a factor of 5 the stress varies by a factor of 45.

TABLE 1 Values of $\bar{U}(19.5)$, $\bar{U}(10)$, u_*^2 and u_* in Meters per Second Except u_*^2 .

$\bar{U}(19.5)$	$\bar{U}(10)$	u_*^2	u_*
5	4.7	0.024	0.156
10	9.5	0.103	0.321
15	14.4	0.281	0.531
20	18.7	0.601	0.775
25	23.2	1.100	1.049

For an air density of 1.25 kg/m^3 , the vector value of $\vec{\tau}$ can be computed along with corresponding parallel and normal estimates of sampling variability.

The finite difference estimate of the curl is given by (17) in units of ($\text{Newtons per square meter}$) per meter.

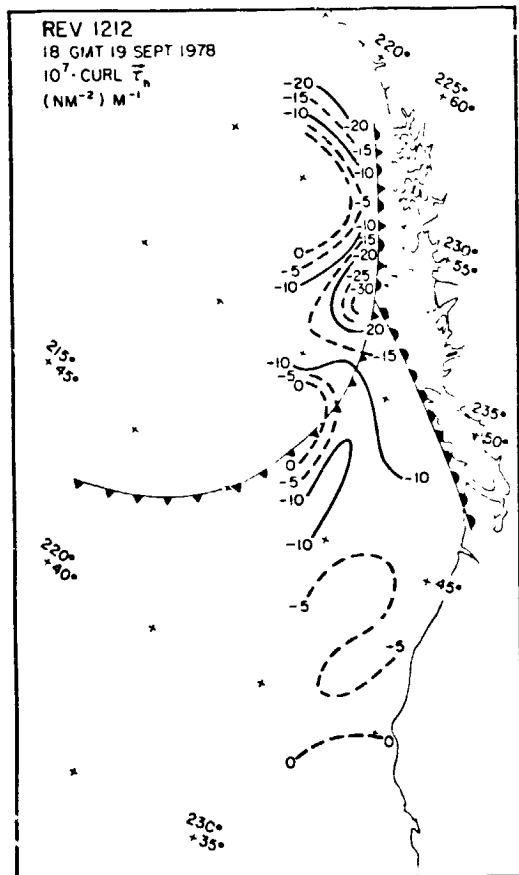


Fig. 4 The Curl of the Wind Stress for REV 1212. Values are in Newtons per Square Meter per Meter.

correct forecast. It is already clear from the analysis of SEASAT products that the specification of wind fields over the oceans can, at times, be grossly in error when only conventional data are used.

$$\text{CURL}(\vec{\tau}_h)_s = \frac{4.5 \cdot 10^{-6}}{\cos \theta_o} \left\{ (\tau_{s\theta}(\lambda_o + 1, \theta_o) - \tau_{s\theta}(\lambda_o - 1, \theta_o)) \right. \\ \left. - \cos \theta_o (\tau_{s\lambda}(\lambda_o, \theta_o + 1) - \tau_{s\lambda}(\lambda_o, \theta_o - 1)) \right. \\ \left. + 0.034905 \sin \theta_o \tau_{s\lambda}(\lambda_o, \theta_o) \right\} \quad (17)$$

ACKNOWLEDGEMENTS

The research reported herein was supported by the National Aeronautics and Space Administration under Contract NAGW-266. We thank the many persons who have helped us as described in the more detailed paper on which this summary is based.

REFERENCES

Bjerknes, V. 1904: Das Problem der Wettervorhersage Betrachtet vom Standpunkte der Mechanik and der Physik, Meteor. Z., Vol. 21, 1-7.

Brunt, D. 1942: Weather Study. The Roland Press Co. 215 pp.

Kirwan, A. D., G. J. McNally, E. Reyna and W. J. Merrell Jr. 1978: The Near Surface Circulation of the Eastern North Pacific. J. Phys. Oceanogr. Vol. 8, No. 6, 937-945.

Large, W. G., and S. Pond 1981: Open Ocean Momentum Flux Measurements in Moderate to Strong Winds. J. Phys. Oceanogr. Vol. 11, 324-326.

McMurdie, L. A., and K. B. Katsaros 1983: Locating Synoptic Fronts and Rain Areas Using the SEASAT Scanning Multichannel Microwave Radiometer. In Studies of Atmospheric Water with the SEASAT Scanning Multichannel Microwave Radiometer. Final Report to NOAA, Cont. Na-81-SAS-00756 U. of Wash. Seattle, Contribution No. 671.

Pierson, W. J. 1983a: The Measurement of the Synoptic Scale Wind Over the Ocean. J. Geophys. Res. Vol. 88 No. C3. 1683-1708.

Pierson, W. J. 1983b: Highlights of the SEASAT-SASS Program: A Review in Allan T. D., Satellite Microwave Remote Sensing. John Wiley and Sons. 69-86.

Pierson, W. J., W. B. Sylvester and R. E. Salfi 1983: Synoptic Scale Wind Field Properties from the SEASAT-SASS. The City College, Tech. Rept. NASA Contract NAGW-266. 152 pp. Plus Appendices.

Pierson, W. J., S. Peteherych and J. C. Wilkerson 1980: The Winds of the Comparison Data Set for the SEAST Gulf of Alaska Experiment, IEEE J. Ocean. Eng. OES(2), 169-176.

Richardson, L. F. 1922: Weather Prediction by Numerical Process, London Cambridge University Press, (Reprinted Dover 1965), 236 pp.

Robinson, G. D 1978: Weather and Climate Forecasting as Problems in Hydrodynamics. M. Weather Rev., Vol. 106, No. 4 448-457.

Woiceshyn, P. M. ed 1979: SEASAT Gulf of Alaska Workshop Vol II Comparison Data Base: Conventional Marine Meteorological and Sea Surface Temperature Analysis. Appendix A and B. JPL Document 622-101. Jet Propul. Lab. Pasadena, Cal.